High-Q Fano resonances in diamond nanopillars

Research Article | Vol. 13, No. 4 / 1 Apr 2023 / Optical Materials Express 1110
Optical Materials EXPRESS

High-Q Fano resonances in diamond nanopillars

VITTORIO BONINO[1,2] AND ANGELO ANGELINI[2,*]

[1]Dipartimento di Scienza Applicata e Tecnologia, Politecnico di Torino, C. so Duca degli Abruzzi 24, Turin 10129, Italy
[2]Advanced Materials and Life Sciences, Istituto Nazionale di Ricerca Metrologica (INRiM), Strada delle Cacce 91, 10135 Turin, Italy
*a.angelini@inrim.it

Abstract: We report on the optical behaviour of a nanostructured diamond surface on a glass substrate. The numerical model reveals that a simple geometrical pattern sustains Fano-like resonances with a Q-factor as high as $3.5 \cdot 10^5$ that can be excited by plane waves impinging normally on the surface. We show that the geometrical parameters of the nanopillars affect both the resonant frequency and the line shape. The nanostructured surface can be straightforwardly used as a refractive index sensor with high sensitivity and linearity. Our findings show that diamond-based meta-surfaces are a valuable nanophotonic platform to control light propagation at the nanoscale, enabling large field enhancement within the nanoresonators that can foster both linear and nonlinear effects.

1. Introduction

In recent years, metasurfaces have demonstrated their capability to drive the evolution of photonic technologies by replacing bulky optical components with ultrathin, integrable, and high-performance devices ready for mass scale production [1]. Metasurfaces consist of a large number of nanoresonators, also known as meta-atoms, whose arrangement influences light scattering, resulting in local modulation of amplitude and phase of the emerging field. By properly choosing the geometrical dimensions, orientation, and material of individual nanoresonators, a high degree of freedom in engineering light scattering can be achieved [2].

This concept has led to the development of several devices to control wavefronts [3], enhance the quality of structural colors [4] enhance and exploit nonlinear effects [5], and provide novel routes to quantum optics [6]. These promising properties have driven the rapid development of metasurfaces, particularly dielectric-based ones and triggered an increasing demand for high refractive index materials with high transparency and large nonlinear coefficients [7,8].

In the visible range there are few materials with such properties, and most of the dielectric photonic nanostructures found in literature are made of silicon [9], silicon nitride [10] and few other high refractive index metal oxides [11] such as hafnium oxide [12] or TiO_2 [13].

Among the dielectric materials, the unique electronic properties of diamond make it extremely interesting for photonic applications. Indeed, on one hand the wide electronic band gap provides an extremely low extinction coefficient and on the other hand diamond exhibits a high refractive index over the entire visible range. The wide electronic bandgap makes diamond an ideal material for hosting more than 500 colour centers, some of which can act as atom-like single photon sources even at room temperature [14,15]. Moreover, diamond exhibits a relatively high nonlinear refractive index ($n_2 = 1.3 \cdot 10^{-19} m^2 W^{-1}$). By gathering all the above mentioned features, diamond results to be a rather promising material for classical and quantum photonic devices [16,17].

Recently, a comprehensive review by Shandilya and coworkers [18] highlighted the potential that diamond has for integrated quantum photonic. However, despite the longstanding interest toward diamond in the quantum optics community, there are still few examples of diamond based metasurfaces in literature, such as metalenses to efficiently extract light from Nitrogen Vacancy

#484614 https://doi.org/10.1364/OME.484614
Journal © 2023 Received 4 Jan 2023; revised 15 Feb 2023; accepted 23 Feb 2023; published 24 Mar 2023

Optical Materials EXPRESS

centers [19], diamond nanostructures sustaining Mie resonances in view of generating artificial colours with high efficiency [20] and nanostructured diamond whose non linear properties have been investigated [21]. The relative lack of diamond based photonic devices is mainly due to the difficulty in growing thin diamond films on substrates different from diamond itself as a consequence of the high surface energy due to strong carbon-carbon bonding [22]. Nevertheless, nucleation-based techniques have been developed to facilitate the growth of diamond, including electrostatic seeding, which is commonly used for nanocrystalline growth [23] or bias enhanced nucleation, which is a primary technique for heteroepitaxial growth [24]. It is worth noting that similar issues related to Silicon based photonics have been solved by the development of Silicon on Insulator (SOI) technology [25], that kicked off the field of integrated photonics, and more recently Silicon Carbide on Insulator technology enabled new photonic devices [26].

In this work, we report on the optical behaviour of diamond nanopillars on a glass substrate. Our numerical model shows that a plane wave impinging normally on the proposed surface pattern can excite Fano-like resonances with a Q-factor as high as $3.5 \cdot 10^5$. To the best of our knowledge this is among the highest values reported in literature for all dielectric metasurfaces [27–30].

We study the dependence of the resonance from geometrical and environmental parameters, showing that both the lineshape and resonant frequency are affected by the height of the pillars and by the refractive index of the external environment. As a direct application of our findings, we show that the diamond metasurfaces can be used as a refractive index sensor with sensitivity up to 72.21 nm per refractive index unit (RIU) and linearity over a wide range of refractive indexes. Our findings shows that diamond-based meta-surfaces are a valuable nanophotonic platform to control light propagation at the nanoscale, enabling large field enhancement within the nanoresonators that can foster both linear and nonlinear effects.

2. Methods

Finite elements method simulation software COMSOL Multiphysics 6.0 has been used to calculate the optical response of the metasurface in the frequency domain. We simulated an infinite array of diamond nanopillars in a square lattice configuration by applying periodic boundary conditions to the unit cell (Fig. 1(a)) along the x and y axes. The unit cell is a square based parallelepiped (lateral side, i.e. the pitch of the array $P = 350nm$, height $3.2\mu m$) and is composed by an individual pillar standing on a glass substrate ($n_{sub} = 1.51$) with diameter $D = 270nm$ and height h that we varied in the simulations from 420 to 660 nm.

An electromagnetic plane wave linearly polarized along the x-direction propagates from the superstrate in the normal direction with respect to the surface. To compute the transmittance profiles we sweeped the frequency with a frequency step $\Delta f = 326GHz$, corresponding to a $\Delta\lambda \approx 0.5nm$. In order to resolve the narrowest resonances, we reduced the frequency step down to $\Delta f \approx 10GHz$ corresponding to a $\Delta\lambda \approx 0.002nm$. We placed two ports at the superstrate and substrate boundaries to calculate transmittance and reflectance. In the first part of the paper, we fixed the superstrate refractive index at 1. In the second part, we varied it from 1 to 1.5. The complex refractive index of diamond as a function of the wavelength is taken from literature [31]. Beside transmittance and reflectance, we can extract and analyze the field distribution inside the pillar along different cross sections.

Optical Materials EXPRESS

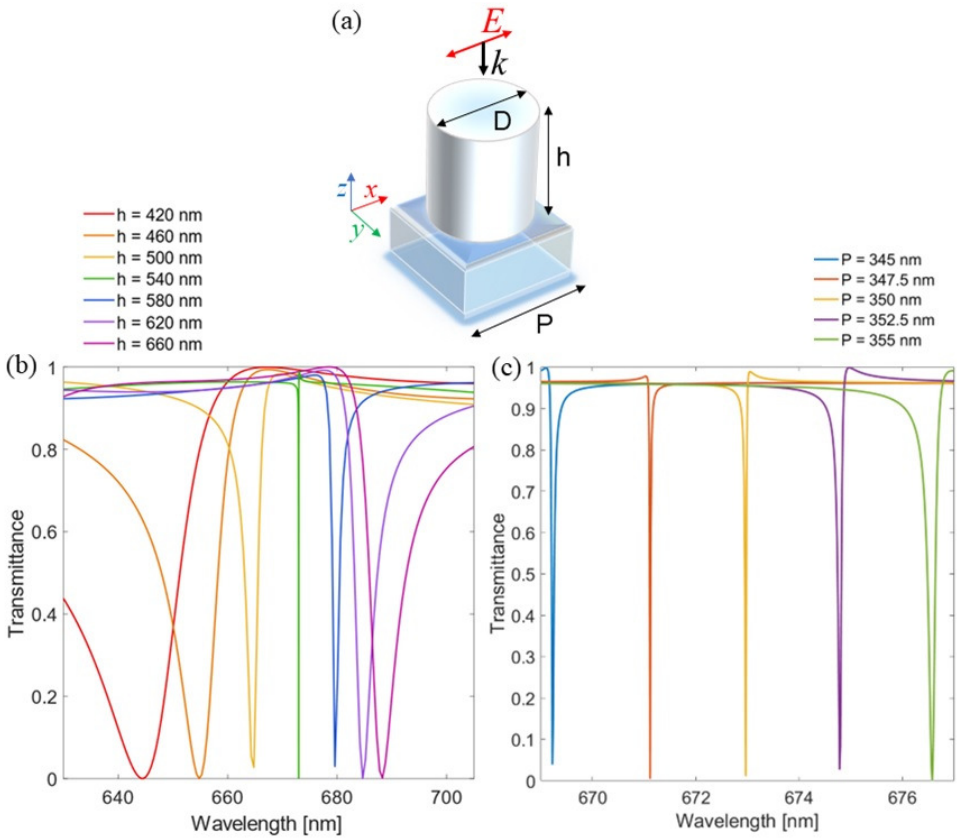

Fig. 1. (**a**) Sketch of the unit cell consisting of a diamond nanopillar on a glass substrate (n = 1.51). The structure is illuminated by an electromagnetic plane wave with a wave vector travelling perpendicular to the surface and linearly polarized along x. Transmittance profiles as a function of incident wavelength for different values of the pillar's height h (**b**) and pitch P (**c**).

3. Results and discussion

Figure 1(b) shows the transmittance calculated for different heights h of the nanopillars. Each profile exhibits a complete suppression of the transmittance at the resonant wavelength, and a red-shift of the resonance is observed upon increase of h. The line width and line shape of the resonances are also strongly affected by the pillar height. An asymmetric profile similar to the typical Fano resonance line shape [32] is clearly observable (red line), and by increasing h we observe a reduction of the asymmetry together with a narrowing of the line width (orange and yellow lines). Above a critical height (green line), the resonance broadens again, and the asymmetric profile appears specular to the previously described ones (blue, violet and purple lines). A similar behaviour is observed when the period of the pillar array is varied (Fig. 1(c)). In particular we observe a blue-shift when the period is reduced, and a red-shift when it is increased. The resonance shift related to the pitch variation suggests a near-field interaction between adjacent pillars.

Firstly, we focus our attention on the Q-factor of the resonance to find out the maximum Q achievable with the proposed geometry. Figure 2(a) shows the profile of the Q-factor as a function

Optical Materials EXPRESS

of h. Here the Q-factor is calculated as follows:

$$Q = \frac{\lambda_r}{\Delta\lambda}, \tag{1}$$

where λ_r is the resonant wavelength and $\Delta\lambda$ is the Full Width at Half Maximum (FWHM). For $h = 500nm$, the Q-factor is $2.9 \cdot 10^2$, while when $h = 542nm$, it reaches $3.5 \cdot 10^4$, revealing an increment of 2 orders of magnitude. For larger values of h the Q-factor decreases again, back to a value of $2.9 \cdot 10^2$ when $h = 600nm$.

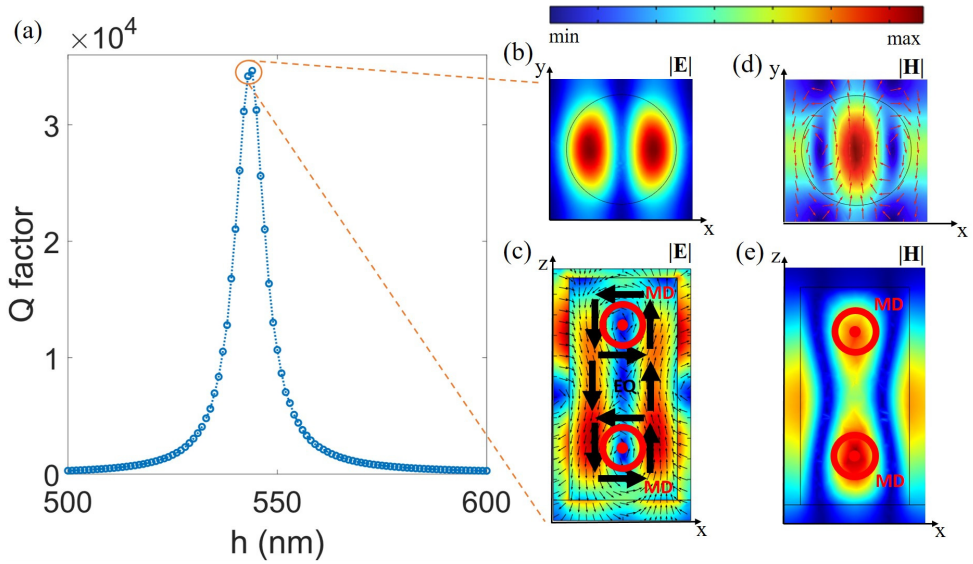

Fig. 2. **a**) Q-factor as function of the height h of the nanopillar, swept from 500 nm to 600 nm. (**b**), (**c**) Norm of the electric field distribution in the xy plane at $z = h/2$ (**b**) and in the xz plane at $y = P/2$ (**c**). (**d**), (**e**) Norm of the magnetic field distribution in the xy plane at $z = 3/4h$ (**b**) and in the xz plane at $y = P/2$ (**d**). The arrows represent electric (black) and magnetic (red) field vectors. The fields are extracted for $h = 540nm$ and wavelength $\lambda = 672.9nm$.

To get some more insights into the resonant behaviour of the diamond nanostructures, we extracted the field distributions when h maximizes the Q-factor (red circle in Fig. 2(a)). The resonant wavelength in this case is $\lambda = 672.9nm$. The full suppression of the forward scattering observed in the transmission spectra and the extremely high Q-factor of the Fano resonances can be understood by looking at the interplay between high order electric and magnetic multipole resonances that satisfies the generalized Kerker condition [33,34]. A recent paper clarified the role of multipole resonances when arrays of nanopillars are considered by performing a multipole expansion analysis on the scattered field [35]. Here, Fig. 2(b) and (c) show the electric field distribution across the xy plane at $z = h/2$ (b) and across the xz plane at $y = P/2$. The electric field is mainly located on the side of the pillar, where it is oriented along z, and outside of it, confirming the near-field coupling between pillars. By looking at the electric field vectors (black arrows in Fig. 2(c)) we observe two closed loops, in the bottom and upper part of the pillar. Both the loops are clockwise, and therefore they generate two magnetic dipole resonances with the magnetic dipole (MD) moment aligned along y. The MD can be clearly seen in Fig. 2(d) and (e). In d, the vectors indicate the orientation of the MD moment. In between the two MDs, the electric field vectors generate an electric quadrupole (EQ) resonance. The overlapping between

Optical Materials EXPRESS

the MD and EQ responses satisfies the condition for the Kerker condition and results in complete suppression of the forward scattering.

To prove that the resonance is a Fano resonance that originates from the overlapping of the background reflected field (bright mode) and the MDs and EQ (dark modes) [4] and to assess the effect of the height of the pillars on the resonance line shape of the resonance we fitted the transmittance spectra with the Fano formula:

$$T(f) = \frac{(\Omega + q)^2)(1 + q)^2}{(\Omega^2 + 1)} \tag{2}$$

where $\Omega = 2 \cdot \frac{f - f_0}{\gamma}$ contains the resonance frequency (f_0) and the resonance width (γ) and q is the Fano parameter [36]. Figure 3(a) shows three transmittance spectra fitted by the Fano

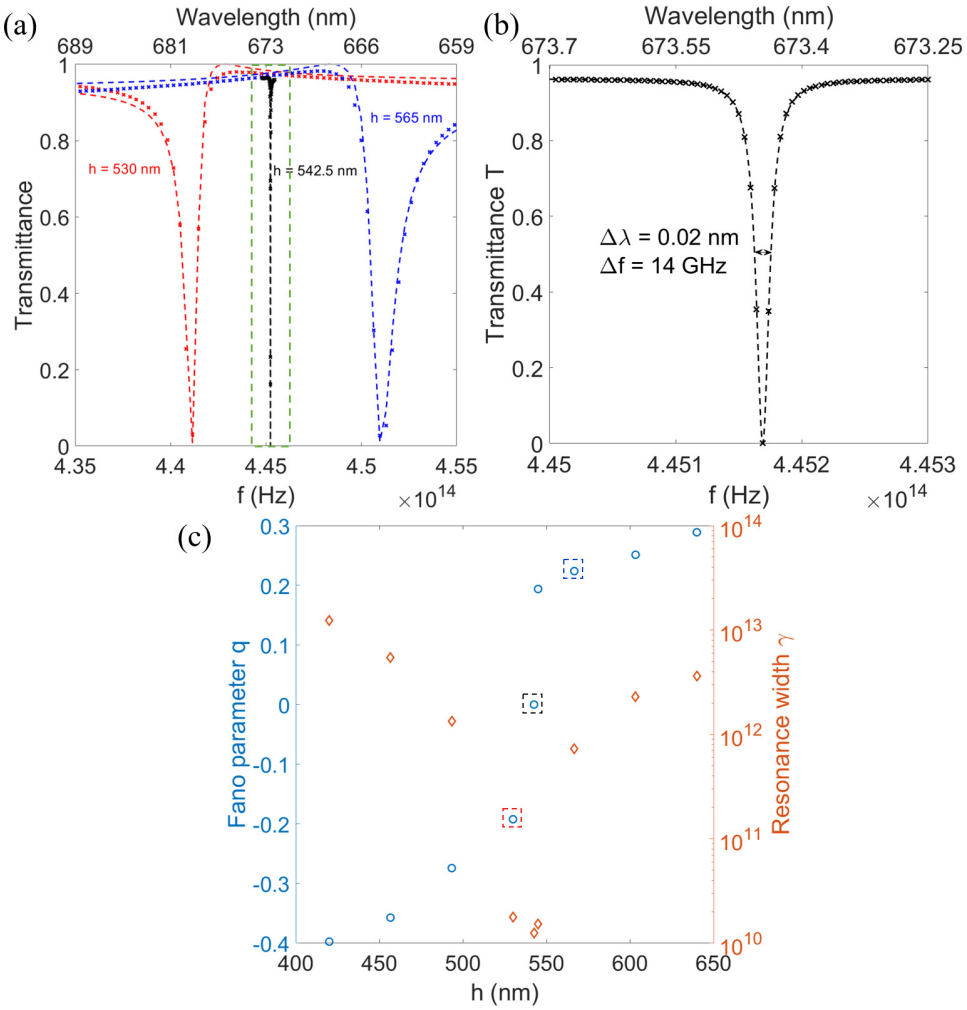

Fig. 3. (**a**) Transmittance as a function of the frequency simulated for different heights of the nanopillars: $h = 520nm$ (red), $h = 542.5nm$ (black) and $h = 565nm$ (blue). (**b**) Transmittance as a function of the frequency simulated for nanopillars with height $h = 542.5$. Δ_λ (Δ_f) is the FWHM of the resonance. (**c**) Fano parameter q and resonance width γ evaluated for different heights of the nanopillars from $h = 400nm$ to $h = 650nm$.

Optical Materials EXPRESS

formula. The red ($h = 530nm$) and blue ($h = 565nm$) curves are slightly detuned from the maximum Q factor condition, while the black one ($h = 542.5nm$) maximises the Q-factor and has been reported in Fig. 3(b) to better evaluate the line shape. The black line has a FWHM $\Delta\lambda = 0.02nm$, which corresponds to a bandwidth $\Delta f = 14GHz$. Figure 3(c) reports the two fitting parameters q - the Fano parameter - and γ as a function of the pillar height. The graph clearly shows a sharp transition of the Fano parameter from negative to positive values, and the red, blue and black dashed squares indicate the points corresponding to the profiles reported in Fig. 3(a). The condition for a Quasi-Lorentzian line shape is achieved when the resonance width (γ) is minimized.

The resonant behaviour of the nanopillars can be exploited for sensing purposes [37]. In order to evaluate the sensitivity and linearity of the diamond-based metasurface with respect to the refractive index of the superstrate, we propose a scenario where the metasurface is fully immersed in a thick homogeneous dielectric material (thickness of the superstrate domain $1.6\mu m$). For the simulation we fixed the height of the pillar at $h = 540nm$ and varied the refractive index of the external layer from 1 to 1.5. The results in Fig. 4(a) show a red shift of the resonant wavelength when n is increased. In Fig. 4(b) we report the position of the resonant wavelength as a function of the external refractive index and the corresponding Q-factor. The induced shift of the resonance is well fitted by a linear function (root mean square error (RMS) = 0.047) with an angular coefficient $S = 72.21nm/RIU$. The Q-factor increases up to $3.5 \cdot 10^5$ when $n_{sup} = 1.25$, corresponding to a FWHM $\Delta\lambda = 0.002nm$. By assuming the FWHM of the resonance as the resolution limit of the system, we can infer that the metasurface can resolve variations of the refractive index up to $4.2 \cdot 10^{-4}$ RIU when the external refractive index is close to 1, and up to $2.73 \cdot 10^{-5}$ RIU when n_{sup} is close to 1.25, as calculated from $\Delta n = \frac{\Delta\lambda}{S}$.

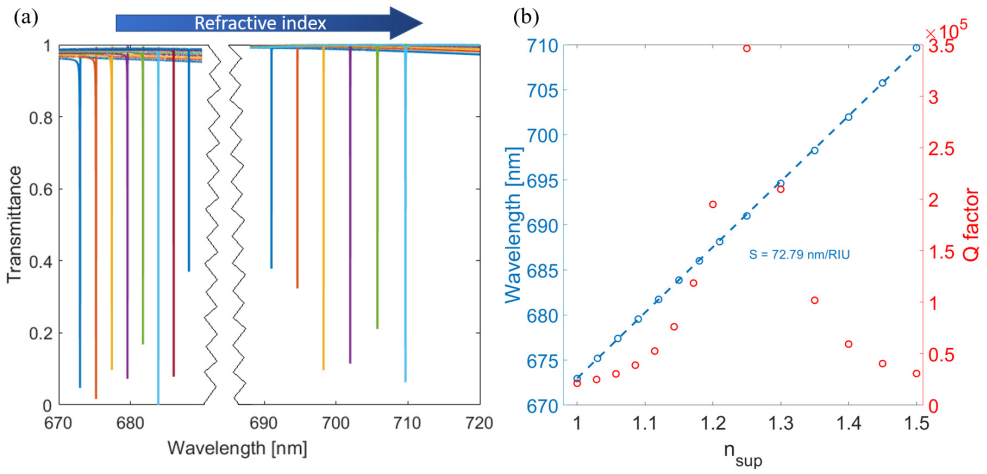

Fig. 4. (**a**) Transmittance spectrum calculated for different refractive index values of the surrounding medium, varying from 1 to 1.5. (**b**) Resonant wavelength as a function of the refractive index of the external medium (blue data, left axis) and Q-factor of the resonance (red data, right axis). The blue data are well fitted by a linear function (blue dashed line) whose slope is S = 72.21 nm/RIU.

4. Conclusions

In this paper we show that an array of diamond nanopillars can be properly engineered to exhibit high Q Fano resonances whose properties can be tuned. We have shown that the quality factor of the resonances is strongly dependent on the height of the individual pillars and periodicity of the

Optical Materials EXPRESS

array, and that the field distribution inside the pillar originates electric and magnetic multipolar moments associated to Mie resonances [38]. By tuning the height of the pillars we match the condition, where the Fano parameters vanishes and the resonance assumes a symmetric lineshape with a Q-factor as high as $3.5 \cdot 10^4$ [36]. We also evaluated the effect of changing the refractive index of the external medium up to a value of 1.5. The change in the environmental refractive index induces a spectral shift of the resonance that is linearly dependent on the refractive index variation, and a resolution down to $2.73 \cdot 10^{-5}$ RIU is theoretically predicted. It is worth notice that excitation and the detection schemes of an eventual sensor is extremely simplified with respect to other optical refractometric sensors based on resonance shift, as for example the Attenuated Total Reflection schemes [39]. In the proposed scheme the white light impinges normally to the surface, making the metasurface based sensor suitable for miniaturization or integration in microfluidic devices. For applications other than sensing such as wavefront shaping or non linear optics, the analysis on the refractive index of the superstrate suggests that the diamond metasurface can be eventually enclosed in a protective low refractive index dielectric layer still preserving a strong resonant behaviour.

Funding. Ministero dell'Università e della Ricerca (2020TS9LXS_004).

Acknowledgments. The authors gratefully thank Dr. Angela Demetriadou from the University of Birmingham for fruitful discussions. We would also like to acknowledge Dr. Paolo Squillari from Politecnico di Torino for technical support with the COMSOL software. The authors acknowledge funding from MUR (Ministero dell'Università della Ricerca) - 2020TS9LXS_004 Polymer mETamateriALs for nanophotonicS (PETALS).

Disclosures. The authors declare no conflicts of interest.

Data availability. Data underlying the results presented in this paper are not publicly available at this time but may be obtained from the authors upon reasonable request.

References

1. "Metasurfaces go mainstream [editorial]," *Nat. Photonics* 17, 02201137 (2023).
2. S. Jahani and Z. Jacob, "All-dielectric metamaterials," Nat. Nanotechnol. **11**(1), 23–36 (2016).
3. W. T. Chen, A. Y. Zhu, V. Sanjeev, M. Khorasaninejad, Z. Shi, E. Lee, and F. Capasso, "A broadband achromatic metalens for focusing and imaging in the visible," Nat. Nanotechnol. **13**(3), 220–226 (2018).
4. O. Hemmatyar, S. Abdollahramezani, Y. Kiarashinejad, M. Zandehshahvar, and A. Adibi, "Full color generation with fano-type resonant hfo2 nanopillars designed by a deep-learning approach," Nanoscale **11**(44), 21266–21274 (2019).
5. N. Nookala, J. Lee, M. Tymchenko, J. S. Gomez-Diaz, F. Demmerle, G. Boehm, K. Lai, G. Shvets, M.-C. Amann, A. Alu, and M. Belkin, "Ultrathin gradient nonlinear metasurface with a giant nonlinear response," Optica **3**(3), 283–288 (2016).
6. T. Stav, A. Faerman, E. Maguid, D. Oren, V. Kleiner, E. Hasman, and M. Segev, "Quantum entanglement of the spin and orbital angular momentum of photons using metamaterials," Science **361**(6407), 1101–1104 (2018).
7. C. Li, P. Yu, Y. Huang, Q. Zhou, J. Wu, Z. Li, X. Tong, Q. Wen, H.-C. Kuo, and Z. M. Wang, "Dielectric metasurfaces: from wavefront shaping to quantum platforms," Prog. Surf. Sci. **95**(2), 100584 (2020).
8. G. Li, S. Zhang, and T. Zentgraf, "Nonlinear photonic metasurfaces," Nat. Rev. Mater. **2**(5), 17010 (2017).
9. I. Staude and J. Schilling, "Metamaterial-inspired silicon nanophotonics," Nat. Photonics **11**(5), 274–284 (2017).
10. Z.-B. Fan, Z.-K. Shao, M.-Y. Xie, X.-N. Pang, W.-S. Ruan, F.-L. Zhao, Y.-J. Chen, S.-Y. Yu, and J.-W. Dong, "Silicon nitride metalenses for close-to-one numerical aperture and wide-angle visible imaging," Phys. Rev. Appl. **10**(1), 014005 (2018).
11. S. M. Choudhury, D. Wang, K. Chaudhuri, C. DeVault, A. V. Kildishev, A. Boltasseva, and V. M. Shalaev, "Material platforms for optical metasurfaces," Nanophotonics **7**(6), 959–987 (2018).
12. M. Zandehshahvar, Y. Kiarashinejad, M. Zhu, H. Maleki, T. Brown, and A. Adibi, "Manifold learning for knowledge discovery and intelligent inverse design of photonic nanostructures: Breaking the geometric complexity," ACS Photonics **9**(2), 714–721 (2022).
13. N. An, K. Wang, H. Wei, and Q. Song, "Fabricating high refractive index titanium dioxide film using electron beam evaporation for all-dielectric metasurfaces," MRS Commun. **6**(2), 77–83 (2016).
14. I. Aharonovich, A. D. Greentree, and S. Prawer, "Diamond photonics," Nat. Photonics **5**(7), 397–405 (2011).
15. I. Aharonovich, D. Englund, and M. Toth, "Solid-state single-photon emitters," Nat. Photonics **10**(10), 631–641 (2016).
16. J. L. Zhang, K. G. Lagoudakis, Y.-K. Tzeng, C. Dory, M. Radulaski, Y. Kelaita, K. A. Fischer, S. Sun, Z.-X. Shen, N. A. Melosh, S. Chu, and J. Vučković, "Complete coherent control of silicon vacancies in diamond nanopillars containing single defect centers," Optica **4**(11), 1317–1321 (2017).

Optical Materials EXPRESS

17. T. Masuda, M. Mitchell, B. Khanaliloo, D. P. Lake, T. Lutz, J. E. Hadden, W. Tittel, and P. E. Barclay, "High-q diamond microdisks for coupling to siv quantum emitters," in *Conference on Lasers and Electro-Optics*, (Optica Publishing Group, 2017), p. JTh3E.2.
18. P. K. Shandilya, S. Flågan, N. C. Carvalho, E. Zohari, V. K. Kavatamane, J. E. Losby, and P. E. Barclay, "Diamond integrated quantum nanophotonics: spins, photons and phonons," J. Lightwave Tech. **40**, 7538 (2022).
19. T.-Y. Huang, R. R. Grote, S. A. Mann, D. A. Hopper, A. L. Exarhos, G. G. Lopez, A. R. Klein, E. C. Garnett, and L. C. Bassett, "A monolithic immersion metalens for imaging solid-state quantum emitters," Nat. Commun. **10**(1), 2392 (2019).
20. J. Jing, Y. C. Yiu, C. Chen, D. Lei, L. Shao, Q. Wang, K. H. Li, N. Wong, and Z. Chu, "A data-mining-assisted design of structural colors on diamond metasurfaces," Adv. Photonics Res. **3**(3), 2100292 (2022).
21. Q. Shen, A. Shams-Ansari, A. M. Boyce, N. C. Wilson, T. Cai, M. Loncar, and M. H. Mikkelsen, "A metasurface-based diamond frequency converter using plasmonic nanogap resonators," Nanophotonics **10**(1), 589–595 (2021).
22. S. Mandal, "Nucleation of diamond films on heterogeneous substrates: a review," RSC Adv. **11**(17), 10159–10182 (2021).
23. O. A. Williams, O. Douhéret, M. Daenen, K. Haenen, E. Osawa, and M. Takahashi, "Enhanced diamond nucleation on monodispersed nanocrystalline diamond," Chem. Phys. Lett. **445**(4-6), 255–258 (2007).
24. S. Yugo, T. Kanai, T. Kimura, and T. Muto, "Generation of diamond nuclei by electric field in plasma chemical vapor deposition," Appl. Phys. Lett. **58**(10), 1036–1038 (1991).
25. A. Rigny, "Silicon-on-insulator substrates: the basis of silicon photonics," https://www.photonics.com/Articles/Silicon-on-Insulator_Substrates_The_Basis_of/a63021(2022). Accessed on Feb. 15, 2023.
26. D. M. Lukin, C. Dory, M. A. Guidry, K. Y. Yang, S. D. Mishra, R. Trivedi, M. Radulaski, S. Sun, D. Vercruysse, G. H. Ahn, and J. Vuckovic, "4h-silicon-carbide-on-insulator for integrated quantum and nonlinear photonics," Nat. Photonics **14**(5), 330–334 (2020).
27. S. T. Ha, Y. H. Fu, N. K. Emani, Z. Pan, R. M. Bakker, R. Paniagua-Domínguez, and A. I. Kuznetsov, "Directional lasing in resonant semiconductor nanoantenna arrays," Nat. Nanotechnol. **13**(11), 1042–1047 (2018).
28. C. Kramer, M. Schäferling, T. Weiss, H. Giessen, and T. Brixner, "Analytic optimization of near-field optical chirality enhancement," ACS Photonics **4**(2), 396–406 (2017).
29. C. Cui, C. Zhou, S. Yuan, X. Qiu, L. Zhu, Y. Wang, Y. Li, J. Song, Q. Huang, Y. Wang, C. Zeng, and J. Xia, "Multiple fano resonances in symmetry-breaking silicon metasurface for manipulating light emission," ACS Photonics **5**(10), 4074–4080 (2018).
30. Z. Liu, Y. Xu, Y. Lin, J. Xiang, T. Feng, Q. Cao, J. Li, S. Lan, and J. Liu, "High-q quasibound states in the continuum for nonlinear metasurfaces," Phys. Rev. Lett. **123**(25), 253901 (2019).
31. H. R. Phillip and E. A. Taft, "Kramers-kronig analysis of reflectance data for diamond," Phys. Rev. **136**(5A), A1445–A1448 (1964).
32. B. Luk'yanchuk, N. I. Zheludev, S. A. Maier, N. J. Halas, P. Nordlander, H. Giessen, and C. T. Chong, "The fano resonance in plasmonic nanostructures and metamaterials," Nat. Mater. **9**(9), 707–715 (2010).
33. R. Alaee, R. Filter, D. Lehr, F. Lederer, and C. Rockstuhl, "A generalized kerker condition for highly directive nanoantennas," Opt. Lett. **40**(11), 2645–2648 (2015).
34. W. Liu and Y. S. Kivshar, "Generalized Kerker effects in nanophotonics and meta-optics [invited]," Opt. Express **26**(10), 13085–13105 (2018).
35. R. Lin, Z. Alnakhli, F. AlQatari, and X. Li, "Analysis of tapered nanopillars for reflective metalens: The role of higher-order modes," IEEE Photonics J. **12**, 1–7 (2020).
36. M. F. Limonov, M. V. Rybin, A. N. Poddubny, and Y. S. Kivshar, "Fano resonances in photonics," Nat. Photonics **11**(9), 543–554 (2017).
37. X. Chen, Y. Zhang, G. Cai, J. Zhuo, K. Lai, and L. Ye, "All-dielectric metasurfaces with high q-factor fano resonances enabling multi-scenario sensing," Nanophotonics **11**(20), 4537–4549 (2022).
38. P. Kapitanova, V. Ternovski, A. Miroshnichenko, N. Pavlov, P. Belov, Y. Kivshar, and M. Tribelsky, "Giant field enhancement in high-index dielectric subwavelength particles," Sci. Rep. **7**(1), 731 (2017).
39. E. Semouchkina, R. Duan, G. Semouchkin, and R. Pandey, "Sensing based on fano-type resonance response of all-dielectric metamaterials," Sensors **15**(4), 9344–9359 (2015).